

Quasi-trapped modes in metasurfaces of anisotropic MoS₂ nanoparticles for absorption and polarization control in the telecom optical range

Alexei V. Prokhorov,^{*,†,‡} Alexander V. Shesterikov,^{†,‡} Mikhail Yu. Gubin,^{†,‡}
Valentyn S. Volkov,[‡] and Andrey B. Evlyukhin^{*,¶,‡}

[†]*Department of Physics and Applied Mathematics, Vladimir State University named after A. G. and N. G. Stoletovs (VlSU), Vladimir, Russian*

[‡]*Center for Photonics and 2D Materials, Moscow Institute of Physics and Technology (MIPT), Dolgoprudny, Russian*

[¶]*Institute of Quantum Optics, Leibniz Universität Hannover (LUH), Hannover, Germany*

E-mail: avprokhorov33@mail.ru; a.b.evlyukhin@daad-alumni.de

Abstract

We investigate the resonant optical response of single material-anisotropic nanoparticles (NPs) of molybdenum disulfide (MoS₂) and their two-dimensional arrays (metasurfaces) irradiated by plane waves of the telecommunication optical range. Nanoparticles in the form of a disk with centered and shifted hole are considered. Using the recently experimental measured the MoS₂ dielectric permittivity and numerical calculations with analytical multipole analysis, we show that the material-anisotropy of NPs can lead to specific nonlocal contributions in their magnetic and electric dipole response and affect

the effective dipole polarizabilities. Applying a special procedure we determine the period of the MoS₂ metasurfaces supporting the quasi-trapped mode (QTM) resonance around the telecom wavelength of 1550 nm. It is shown that regardless extremely weak absorption of the single nanoparticles, the excitation of the QTM leads to effective narrowband absorption in the metasurfaces. Influences of the linear polarization direction of normally incident waves on the QTM implementation and the reflection and transmission spectra are studied. It is found and demonstrated, for the first time, that a metasurface, composed of the MoS₂ disks with their anisotropy perpendicular to the metasurface plane, has the properties of a continuous birefringent medium. Due to these properties, normally incident and linear-polarized waves can be transformed in the transmitted and reflected waves with changed polarizations.

Keywords

anisotropic materials, bianisotropic nanoparticles, all-dielectric metasurface, quasi-trapped mode, collective absorbing, polarization transformation

1 Introduction

Currently, the design of the ultra-narrowband absorbers is of great practical interest. Until recently, the structures and metasurfaces based on the conductive materials have been used to create such absorbers. The configuration and lattice resonances in them allow narrowing the spectral transmission window, while the conductor provides a fast damping of light in it.¹⁻⁴ The composite metal-dielectric absorbers utilize the resonances of a dielectric metamaterial in order to concentrate a light and direct it to a plasmonic substrate for conversion of near field energy to Joule losses.⁵ The quality factor of the considered resonances as the ratio of the resonant wavelength to the full width at half maximum (FWHM) depends on the topology of the structure. For example, in Ref. 3 using gold mushrooms on a complex substrate, the

quality factor is about 130 in the near-infrared range; in the theoretical work⁴ for an array of gold nanoribbons on a thin gold layer, it reaches 350 in the visible range. In addition, the terahertz absorbers based on the structured graphene⁶ with quality factor of about 9 and with quality factor of about several hundred units⁷ for a wavelength 1550 nm were proposed. An additional remarkable feature of narrowband absorbers is high sensitivity to the local environment, which allows to detect individual particles and nanoobjects with high precision.^{8–11} However, the obligatory presence of a plasmon substrate in such structures allows to use them only as individual devices of limited size. In the case of creating the spatially distributed sensor of a large size or depositing the absorbing coating on a flexible substrate of arbitrary shape, the presented approach is not applicable. Partial solution can be the use of nanoparticle (NP) lattice without plasmonic substrate and the utilizing absorption properties of the NPs forming the lattice. In this case the diffractive-coupled lattice of metal or semiconductor NPs provides the collective lattice resonances with the quality factors determined by the configuration and size perimeters of the system.^{12–17}

The recent researches have focused on the development of all-dielectric absorbers and sensors, for which a high level of absorption is achieved by matching impedances and combining electric and magnetic dipole resonances at the same frequency in a metamaterial fabricated from weakly absorbing NPs, for example, solid Si NPs.^{18,19} However, the quality factor of such systems is low and does not exceed 12. Not very high values of quality factor are reached in metasurfaces composed of doped Si building blocks with increased material losses, see Refs. 20–22.

The improvement of quality factor control of the all-dielectric absorbers and enhancing sensitivity of the corresponding sensors can be reached, on the one hand, applying new physical mechanism, and, on the other hand, using new optical materials for their fabrication. One such an approach is to use the combination of the fundamental effects of nonlocality in single NPs optical response and the collective resonances²³ in all-dielectric metasurfaces composed of such building blocks.^{24,25} In particular, the metasurface composed of optically

bianisotropic NPs²⁶ can support the quasi-trapped modes (QTM) or, by other words, the quasi bound states in the continuum (q-BICs).²⁷ In general the trapped modes or BICs are protected eigenmodes of ideal lossless optical systems remaining perfectly localized without radiation into free space²⁸ that provides their infinite Q-factor resonances and perfect confinement of optical energy.^{29–31} In practical cases, access to similar states can be obtained by weak distortion or perturbation of ideal structure’s symmetrical properties that converts the trapped modes into QTM (q-BICs).^{32,33} For metasurfaces such perturbations can be realized via exploiting of especially initiated bianisotropic properties of their building blocks.

Recently, it was analytically demonstrated in Ref. 34 that, in the metasurfaces composed of dielectric nanodisks with an eccentric through hole, the QTM are generated due to the self-synchronization for the single disk’s magnetic dipole moments oriented orthogonally to the metasurface and excited due to the disk’s bianisotropic response. The strength of this effect depends on the values of the nondiagonal elements of the disk’s dipole polarizability tensor that is responsible for the bianisotropy.^{26,34} In the case of the QTM excitation, the transmission and reflection spectra of arrays of such particles have the ultra-narrow resonances^{33,34} which can be associated with the nonlinear³⁵ and absorption (thermal)³⁶ processes.

So far the referenced results related with QTM concerned the metasurfaces composed of nanoparticles with isotropic dielectric properties. In these cases, for realization of the required resonances of single particles only shape and size factors can be applied. However, the use of 2D layered anisotropic materials³⁷ such as MoS₂^{38–42} for metasurface’s building blocks can provides an additional degree of freedom for tuning and control of their optical resonances. Due to the considerable difference between the refractive indices along and orthogonal to the material layers, their resonant response can be significantly sensitive to the propagating and polarization properties of incident light waves. This is of fundamental importance, since the higher dielectric anisotropy of single nanoparticles in metasurfaces can result in new possibilities with respect to the excitation and manipulations of the QTM

leading to the selective resonant light absorption, transmission, or reflection. In order to clarify and demonstrate these new facilities, in this article we investigate the features of the trapped mode realization in the metasurfaces composed of MoS₂ disk particles. We show that, due to the QTM response of such metasurfaces, an effective narrow absorption band can be realized in the telecom (wavelength ~ 1550 nm) spectral range, where MoS₂ material has very weak anisotropic absorption. Besides, the influence of the polarization rotation of the incident field, relative to the orientation of MoS₂ layers in the disks, on polarization changes of transmitted and reflected waves is investigated.

2 Resonant absorption in MoS₂ metasurfaces

In this article, we will consider metasurfaces composed of disk nanoparticles made of MoS₂ with layers perpendicular to the disk base and parallel to the yOz plane (Figure 1a). Every disk has radius R_2 , height H and a through hole with radius R_1 . The hole can be shifted on Δ along y -axis, as it is shown in Figure 1a. The normal irradiation conditions are shown also in Figure 1a, where $E = (E_x, 0, 0) \exp(ikz)$ ($H = (H_y, 0, 0) \exp(ikz)$) are the incident electric and magnetic fields, \vec{k} is the wave vector of the normally incident plane wave.

2.1 Optical properties of single disks

Since the properties of metasurfaces are determined by the combinations of single particles resonances and the collective resonances of total structure, we start from a detail discussion the question how the anisotropy of MoS₂ dielectric permittivity,³⁸ affects the scattering of light by the single MoS₂ disks with the symmetric through hole. In the Cartesian coordinate

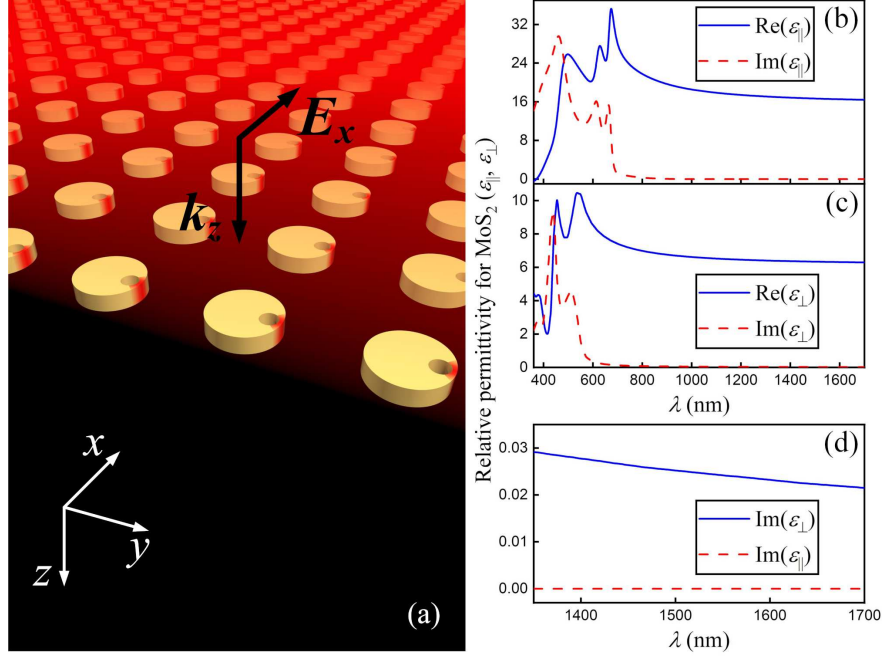


Figure 1: (a) The model of metasurface composed of hollow MoS₂ disks with visualization of the electric field component in the regime of quasi-trapped mode generation stylized on the base of numerical simulation. Relative dielectric permittivity for MoS₂ (b) along and (c) orthogonal to the material layers.³⁸ (d) The comparison of imaginary parts of permittivities for mutually orthogonal directions.

system shown in Figure 1a the tensor of MoS₂ dielectric permittivity $\hat{\epsilon}_p$ is written as

$$\hat{\epsilon}_p = \begin{pmatrix} \epsilon_{\perp} & 0 & 0 \\ 0 & \epsilon_{\parallel} & 0 \\ 0 & 0 & \epsilon_{\parallel} \end{pmatrix}, \quad (1)$$

where the values of ϵ_{\perp} and ϵ_{\parallel} have been recently measured^{38,41} and shown in Figure 1b,c. For calculations of the scattering cross sections and corresponding their multipole decompositions we apply the following approach: the electric and magnetic fields, induced polarization and density of the displacement current inside the scatterers are calculated using the COMSOL facilities for the problem of light plane wave scattering by a finite-size target, and then the contributions of the main multipole moments into the scattering cross section σ_{scat} are

determined from the expression:⁴³

$$\begin{aligned}
\sigma_{scat} \simeq & \frac{k^4}{6\pi\varepsilon_0^2|\mathbf{E}|^2}|\mathbf{p}|^2 + \frac{k^4\varepsilon_d\mu_0}{6\pi\varepsilon_0|\mathbf{E}|^2}|\mathbf{m}|^2 \\
& + \frac{k^6\varepsilon_d}{720\pi\varepsilon_0^2|\mathbf{E}|^2}\sum_{\alpha\beta}|Q_{\alpha\beta}|^2 + \frac{k^6\varepsilon_d^2\mu_0}{80\pi\varepsilon_0|\mathbf{E}|^2}\sum_{\alpha\beta}|M_{\alpha\beta}|^2 \\
& + \frac{k^8\varepsilon_d^2}{1890\pi\varepsilon_0^2|\mathbf{E}|^2}\sum_{\alpha\beta\gamma}|O_{\alpha\beta\gamma}|^2,
\end{aligned} \tag{2}$$

where k is the vacuum wave number, ε_0 and ε_d are the vacuum dielectric constant and relative dielectric constant of surrounding medium, respectively, μ_0 is the vacuum permeability, \mathbf{E} is the vector electric amplitude of the incident plane waves, \mathbf{p} and \mathbf{m} are the vectors of electric and magnetic dipole moments of the scatterer, respectively, and \hat{Q} , \hat{M} , and \hat{O} are the tensors of electric and magnetic quadrupole moments, and electric octupole moment, respectively. Corresponding expressions for the multipole moments defined by the density of the displacement current can be found elsewhere.⁴³ In this article we consider that the all multipole moments of single nanoparticles is located at their center of mass. This also concerns the calculation of the dipole polarizabilities presented further.

The scattering cross sections for different irradiation conditions are shown in Figure 2. Independently on these conditions the scattering in the telecom optical range ($\lambda \in [1250 - 1650]$ nm) is basically determined by electric dipole (ED) and magnetic dipole (MD) moments of the disk. For normal incidence of the plane waves along z -axis (Figure 2a and 2c) one can see strong influence of the incident wave polarization on the spectral positions of ED and MD resonances caused by the MoS₂ dielectric anisotropy. Changing the electric polarization from E_x (being perpendicular to MoS₂ layers, Figure 2a) to E_y (being parallel to MoS₂ layers, Figure 2c), the value of the cross section increases and the dipole resonances are shifted to the “red” side. For the E_y -polarization (electric field is directed along the layers), the resonant MD contribution considerably increases. In this case, the MD moment is directed perpendicular to the layers and determined by the ring displacement current induced in

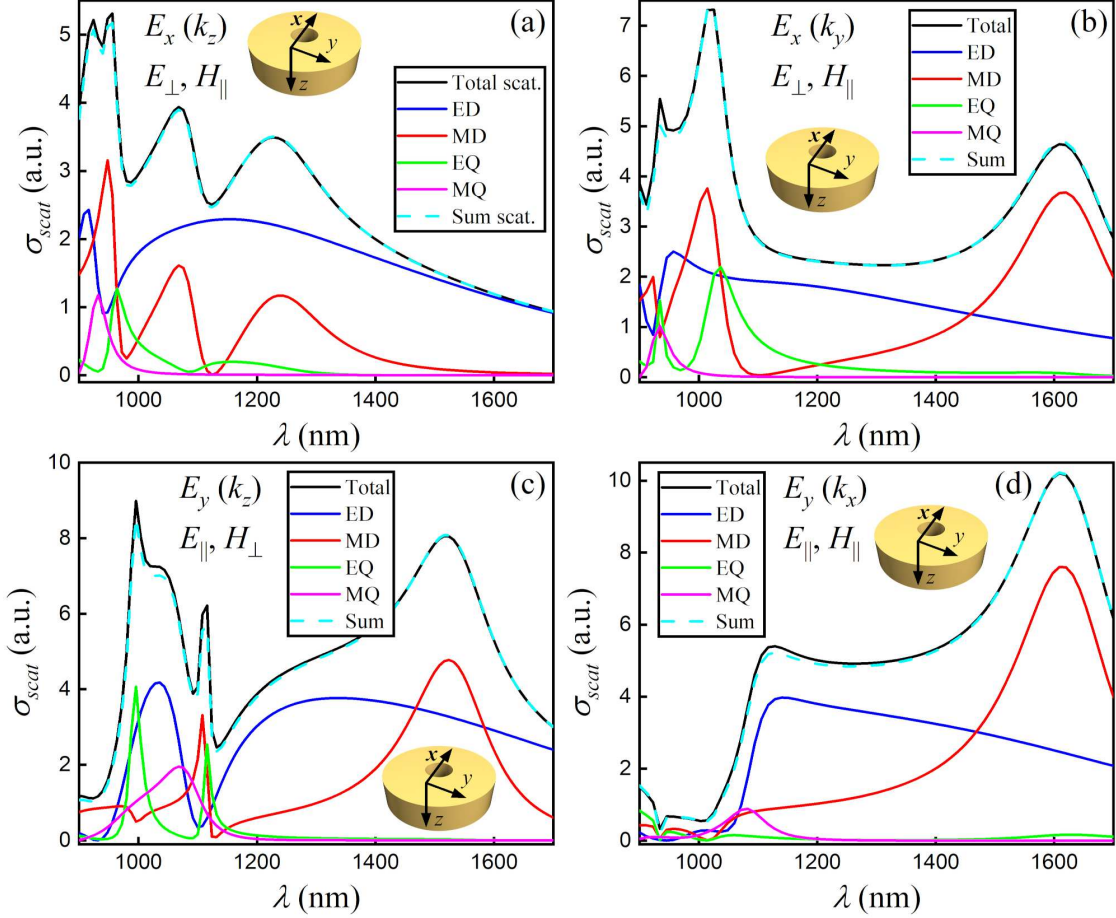


Figure 2: Spectra of the scattering cross sections with corresponding multipole decomposition calculated for the MoS₂ disk (the radius and height $R_2 = H = 258$ nm) with the central through hole (the radius $R_1 = 82$ nm) and for different irradiation conditions clarified by the insets. Orientation of the MoS₂ layers is parallel to yz -plane.

these layers characterized by a large refractive index $n \sim \sqrt{\epsilon_{||}}$. The "red" shift follows from the estimation of the wavelength λ_{res}^{MD} corresponding to the MD resonance of a dielectric particle with dimension D and having refractive index n : $\lambda_{res}^{MD} \sim Dn$ - for fixed D , the resonant wavelength increases with n . Thus, the normally propagating light waves with E_x -polarization (perpendicular to the layer) do not excite resonant response of the disks around $\lambda = 1500$ nm, in contrast to the case of the orthogonal E_y -polarization.

For the side irradiation and H_z -polarization the results are presented in Figures 2b and 2d. One can see that the spectral position of the first MD resonance ($\lambda = 1620$ nm) does not almost depend on the orientation of the external electric field, whereas the values of the

corresponding scattering cross sections are different: for the electric field being parallel to the MoS₂ layers the scattering cross section is larger owing to larger value of the induced displacement current in xy -plane. In this case, the value of the resonant MD at $\lambda = 1620$ nm is also larger than for other case shown in Figure 2b. Due to symmetry properties of the disk the MD excited by the side irradiation with H_z -polarization has the only m_z component for which

$$|m_z^{\parallel}| > |m_z^{\perp}|, \quad (3)$$

where $m_z^{\parallel(\perp)}$ is the MD z -component for the side irradiation with electric field polarization parallel (perpendicular) to the MoS₂ layers. The inequality (3) is followed from the anisotropy of $\hat{\varepsilon}_p$ which also results in the nonlocal optical response of the MoS₂ disk.

In the dipole approximation with inclusion of the first-order nonlocal response, the electric and magnetic dipole moments of single NPs irradiated by an external wave with electric \mathbf{E} and magnetic \mathbf{H} fields can be written in the form⁴⁴

$$\mathbf{p} = \hat{\alpha}^{ee}\mathbf{E} + \hat{\alpha}^{em}\mathbf{H} + \hat{a}[\nabla \otimes \mathbf{E}], \quad (4)$$

$$\mathbf{m} = \hat{\alpha}^{mm}\mathbf{H} + \hat{\alpha}^{me}\mathbf{E} + \hat{c}[\nabla \otimes \mathbf{E}], \quad (5)$$

where $\hat{\alpha}^{ee(mm)}$ is the tensor of electric (magnetic) dipole polarizability corresponding to the direct (local) excitation of the dipole moment by the electric (magnetic) field of the incident wave. The second and third terms in Equations (4) and (5) correspond to the bianisotropic and next nonlocal, respectively, excitation of \mathbf{p} and \mathbf{m} . From the reciprocity property of the considered scattering systems the tensors of bianisotropic polarizabilities satisfy the following relation: $\mu_0 \hat{\alpha}^{me} = -(\hat{\alpha}^{em})^T$,⁴⁵ where T denotes the transpose operation. Moreover, from the deriving of (4) and (5),⁴⁶ the elements of the tensors \hat{a} and \hat{c} satisfy the following symmetry properties: $a_{ijl} = a_{ilj}$ and $c_{ijl} = c_{ilj}$. Further, we will consider that, when the orientation of the excited dipole is collinear with the wave vector of the incident wave, the bianisotropy is longitudinal, and when it is perpendicular, the bianisotropy is transverse.

Note that all tensor coefficients in (4) and (5) depend only on geometrical and materials characteristics of scatterers and are independent on irradiation conditions.

2.2 Dipole polarizabilities of single nanoparticles

In order to determine the conditions of resonant coupling between NPs periodically arranged in metasurface (as shown in Figure 1), one needs to know certain components of the tensor coefficients from (4) and (5) which correspond to the lateral irradiation of the single disk. They can be obtained from (4) and (5), if the dipole moments \mathbf{p} and \mathbf{m} of NP are known from numerical calculations for the two separate irradiation conditions (along x - and y -direction). For example, in the case of studying coupling effects with a magnetic dipole moments being perpendicular to the metasurface plane, it is convenient to get from (4) the system of equations in the form:

$$m_z^{(k,E,H)} = \alpha_{zz}^{mm} H_z + c_{zyx} i k E_y + \alpha_{zy}^{me} E_y, \quad (6a)$$

$$m_z^{(-k,E,-H)} = -\alpha_{zz}^{mm} H_z - c_{zyx} i k E_y + \alpha_{zy}^{me} E_y, \quad (6b)$$

$$m_z^{(E,k,-H)} = -\alpha_{zz}^{mm} H_z + c_{zxy} i k E_x + \alpha_{zx}^{me} E_x, \quad (6c)$$

$$m_z^{(E,-k,H)} = \alpha_{zz}^{mm} H_z - c_{zxy} i k E_x + \alpha_{zx}^{me} E_x. \quad (6d)$$

The Equations (6a) and (6b) correspond to the irradiation of NPs in two opposite directions: forward and backward to the Ox axis, while maintaining the direction of the vector \mathbf{E} along Oy axis. This information is indicated by the superscripts for m_z . The Equations (6c) and (6d) correspond to the irradiation in forward and backward directions along Oy axis while maintaining the direction of the vector \mathbf{E} along Ox axis (see the corresponding superscripts for the moment). Using the symmetrical property $c_{zxy} = c_{zyx}$, the solution of system (6) in

the general case, have the form:

$$\alpha_{zz}^{mm} = \frac{1}{4H_z} \left[(m_z^{(k,E,H)} - m_z^{(-k,E,-H)}) + (m_z^{(E,-k,H)} - m_z^{(E,k,-H)}) \right], \quad (7a)$$

$$c_{zxy} = \frac{1}{2ik(E_x + E_y)} \left[(m_z^{(k,E,H)} - m_z^{(-k,E,-H)}) - (m_z^{(E,-k,H)} - m_z^{(E,k,-H)}) \right]. \quad (7b)$$

Note that due to inverse symmetry of the MoS₂ disk NP⁴⁷ there is no bianisotropy, but a nonlocal response can be excited. This result is a consequence of the anisotropy of NP material since for these irradiation conditions this effect is not observed in isotropic disks⁴⁷ for which the magnetic dipole component m_z is determined only by the local term with α_{zz}^{mm} in (6). Formally, we can also include the nonlocal response in effective polarizabilities (which become dependent on irradiation conditions) defining them as

$$\alpha_{zz}^{mm(x)} = \frac{m_z^{(k,E,H)}}{H_z} \quad \text{and} \quad \alpha_{zz}^{mm(y)} = \frac{m_z^{(E,-k,H)}}{H_z} \quad (8)$$

under the irradiation with a wave vector that is collinear to the Ox and Oy axes, respectively. Note that such effective polarizabilities of isotropic disks with a dipole response coincide with their direct polarizabilities α_{zz}^{mm} . The inverse values of the corresponding polarizabilities calculated for the disk NP with the central hole as in Figure 2 are presented in Figure 3 for different incident wavelengths λ . The curves corresponding to the direct (local) dipole polarizability α_{zz}^{mm} and its effective counterparts $\alpha_{zz}^{mm(x)}$ and $\alpha_{zz}^{mm(y)}$ significantly differ because of the nonlocal response additions. Note that the intersection point of the real parts of the inverse direct (local) and effective polarizabilities corresponds to their zero values coinciding with the magnetic-dipole resonant condition $\text{Re}(1/\alpha_{zz}^{mm}) = 0$ realized at the telecom wavelength $\lambda = 1607$ nm, see Figure 3. At the same time, the imaginary parts of $1/\alpha_{zz}^{mm(x)}$ and $1/\alpha_{zz}^{mm(y)}$ do not coincide in all considered spectral range including the resonant condition, which leads to the difference in the values of the dipoles $m_z^{(k,E,H)}$ and $m_z^{(-k,E,-H)}$ and, therefore, to different energies of their excitation.

In the region of small wavelengths around $\lambda = 950$ nm a considerable difference in the

scattering cross sections, shown in Figure 2, appears due to anisotropic properties of the disk and high-order multipoles excitation. However, in our further consideration we shall concentrate our attention only on the telecom long-wavelength region where the NP optical properties are determined only by their dipole response.

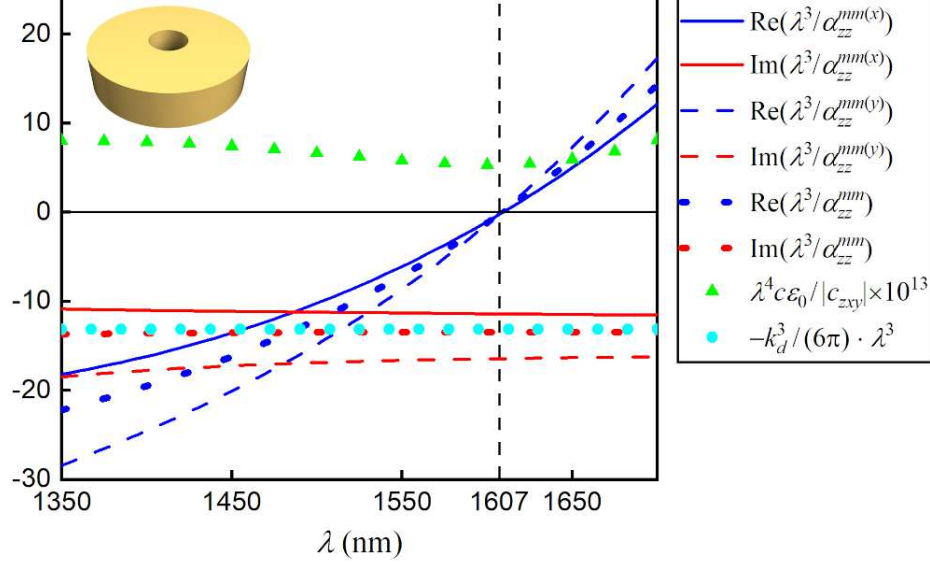


Figure 3: Real (blue curves) and imaginary (red curves) parts of inverse polarizabilities and nonlocal response (green triangles) calculated according to (7) for α_{zz}^{mm} (dotted curves) and derived from equations (6a)–(6b) for the effective $\alpha_{zz}^{mm(x)}$ (solid curves) and $\alpha_{zz}^{mm(y)}$ (6c)–(6d) (dashed curves), separately, for lossless MoS₂ disk with radius and height $R_2 = H = 258$ nm with centered symmetric hole with radius $R_1 = 82$ nm shown in the inset. The cyan circles correspond to the analytical expression (11b) for the dipole sum.

2.3 Quasi-trapped modes of MoS₂ metasurfaces

According to (4) and (5) under $E = (E_x, 0, 0)\exp(ikz)$ irradiation conditions, the electric and magnetic dipole moments excited in a single disk NP can be determined as follows:

$$p_i = \alpha_{ix}^{ee} E_x + \alpha_{iy}^{em} H_y + a_{ixz} ik E_x, \quad (9a)$$

$$m_i = \alpha_{iy}^{mm} H_y + \alpha_{ix}^{me} E_x + c_{ixz} ik E_x, \quad (9b)$$

In the case $i = z$, second terms correspond to the longitudinal bianisotropy, which can be used for excitation of the quasi-trapped modes of the metasurface composed of such disks, as it has been discussed in Ref. 34. The bianisotropic response of the single disk can appear due to the violation of its inverse symmetry, which is achieved, for example, by shifting a hole on a value Δ_y along the in-plane Oy axis of the Cartesian coordinate system, see inset in Figure 4a. In this case, the magnetic-type longitudinal bianisotropy, leading to m_z , is associated with the term $\alpha_{zx}^{me} E_x$ in (9). Note that in order to obtain the longitudinal bianisotropy of the electric type, leading to p_z , it is sufficient to change the polarization of the incident wave from E_x to E_y .

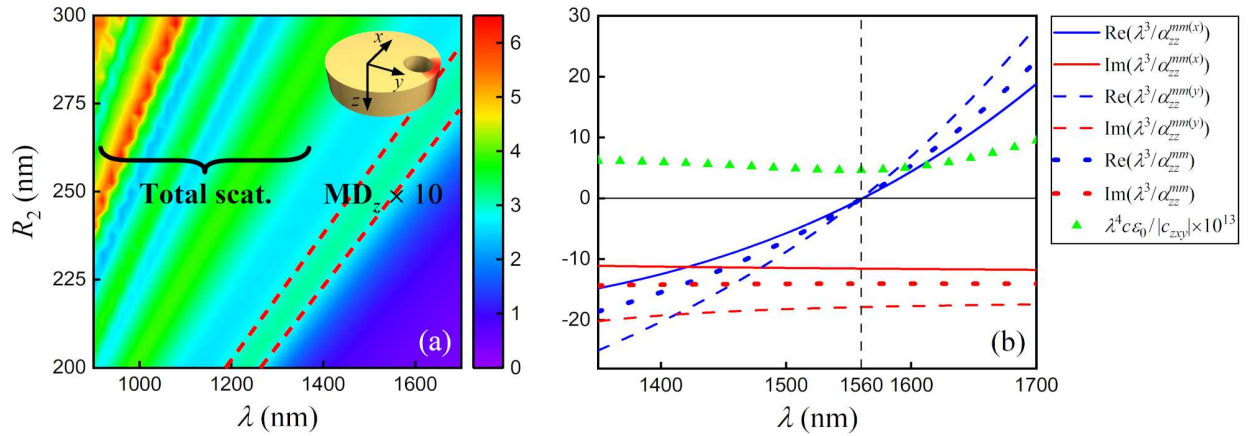


Figure 4: (a) The contour plot on the parametric plane (λ ; R_2) for total scattering cross sections and the partial scattering cross-section associated only with MD component m_z (MD_z) calculated for MoS₂ disks with an eccentric hole normally irradiated by linear E_x -polarized waves. The hole with radius $R_1 = 0.318R_2$ is shifted on $\Delta_y = 0.38R_2$, inset in (a) shows the position of the shifted hole in a disk relative to the axes of the Cartesian coordinate system and schematic illustration of hot spot for near field E_x . The disk's height $H = R_2$. (b) the same that in Figure 3, but for the disk with this shifted hole.

Spectral positions of multipole resonances of single dielectric disks can be tuned by variation of their geometrical parameters.^{48,49} For the MoS₂ disks with hole shifted along MoS₂ layers with $\epsilon_{||}$ (along the y -axis) and normally irradiated by plane waves with electric field $E = (E_x, 0, 0)\exp(ikz)$, the results of such tuning procedure are shown in Figure 4a. This figure presents the contour plot of the scattering cross sections of MoS₂ disks with $H = R_2$, $R_1 = 0.318R_2$ and $\Delta_y = 0.38R_2$ over the parametric plane (λ ; R_2). For convenience of the

result analysis, Figure 4a also includes separate contributions of m_z into the total scattering cross sections excited due to the bianisotropic response with α_{zx}^{me} . One can see that with an increase of the disk radius, its resonances, including the resonant m_z contribution, shift to longer wavelengths. Note that the bianisotropic resonance m_z has a spectral position separated from the main resonances. The importance of this behaviour will be seen from further consideration. Note that the redshift of m_z resonance is solely due to the orientation of the MoS₂ layers relative to the incident field. In particular, the wavelength of the main scattering resonances for a disk is proportional to its effective permittivity. Since the layers are arranged perpendicular to the exciting field E_x , this effective permittivity is mainly determined by the component ε_{\perp} . Taking into account that $\varepsilon_{\parallel} > \varepsilon_{\perp}$, the main resonances are in the region of short wavelengths, see Figure 4a.

In order to have the bianisotropic m_z resonance in the middle of the telecom range we choose the disks with $R_2 = 258$ nm and $H = 258$ nm for the formation of metasurfaces. The disks of such sizes have been studied in Subsection 2.1, where the dependence of the spectral positions of their main optical resonances on the irradiation conditions were explained. That obtained results also qualitatively correspond (excluding the bianisotropy) to the disks with shifted hole because the shift can be considered as a weak perturbation.

Before to study optical properties of metasurfaces composed of the MoS₂ disks with bianisotropic response, let us discuss some general positions related to existence and excitation of BICs in metasurfaces composed of dipolar particles. As it has been discussed in Refs. 34,50, in the case of zero ohmic losses, the collective effect of synchronization of individual magnetic moments m_z in an infinite periodic array of holey isotropic disks (with the dipole response) placed in xOy plane with the period P can lead to the formation of BICs in the regime of trapped mode realization. If the magnetic dipole moment m_z is associated only with the direct dipole polarizability α_{zz}^{mm} , the condition of the trapped mode existence corresponds

to the solution of the transcendental equation in the form:^{34,50}

$$S_z^{(R)} = \text{Re} \left(\frac{1}{\alpha_{zz}^{mm}} \right), \quad (10)$$

where $S_z^{(R)}$ is the real part of the dipole sum $S_z = S_z^{(R)} + iS_z^{(I)}$ with infinite number of terms.

Its parts can be determined as follows:

$$S_z^{(R)} = \frac{k_d^2}{4\pi} \sum_{l,j} \left(\frac{\cos(k_d d_{lj})}{d_{lj}} - \frac{\sin(k_d d_{lj})}{k_d d_{lj}^2} - \frac{\cos(k_d d_{lj})}{k_d^2 d_{lj}^3} \right), \quad (11a)$$

$$S_z^{(I)} = -\frac{k_d^3}{6\pi}, \quad (11b)$$

where the last equality is obtained in the non-diffractive regime for which the period P of the array is smaller than the incident wavelength so that $k_d P < 2\pi$. Here, the parameter $d_{lj} = P\sqrt{l^2 + j^2}$ is the distance from the Cartesian coordinate system origin, coinciding with position of a lattice node, to all other nodes of the lattice which are numbering by indices l and j , $k_d = 2\pi/\lambda_d$, and λ_d is the incident wavelength in the surrounding medium with relative dielectric constant ε_d . In this paper we consider that $\varepsilon_d = 1$.

Using (10) and (11a) together with α_{zz}^{mm} , it is possible to determine the lattice period P for a given wavelength of trapped mode λ_{TM} .⁵¹ For example, we can fix the single particle polarizability α_{zz}^{mm} at a certain wavelength (λ_{TM}) and then, solving (10), to find the period P of a metasurface (with a square elementary cell) that will support the trapped mode state at this λ_{TM} . Note, since the imaginary part $S_z^{(I)}$ of the dipole sum in (11b) does not depend on the lattice period P , the Equation (11b) is always correct in the non-diffractive regime. Let's consider the equation

$$S_z^{(I)} = \text{Im} \left(\frac{1}{\alpha_{zz}^{mm}} \right), \quad (12)$$

providing together with Equation (10) the second condition for the existence of a symmetry protected bound state in the continuum or, by other words, a true trapped mode with infinite quality factor. However, the condition (12) can be exact satisfied only in the case of

the dipole response without ohmic losses, when $\text{Im}(1/\alpha_{zz}^{mm}) = -k_d^3/(6\pi)$.^{34,50}

In general, the electric and magnetic dipole moments of NPs can include the contributions stemming on the nonlocality including the bianisotropy, see Equations (4) and (5), and the absorption. In these cases, the metasurfaces composed of such dipole NPs cannot support the ideal BICs, but there can be realized so-called q-BICs or QTMs characterized by finite quality factors, the values of which are determined by the bianisotropy contributions. However, as shown our calculations, even in the cases of the nonlocality, the relation (10) only with α_{zz}^{mm} , can be used for determination of the lattice period P of the metasurface supporting a QTM at λ_{TM} . We assume that this follows from the fact that only dipole-dipole interaction is involved in the QTM formation, while a nonlocal response can be related with the generation of scatterer dipole moments by high order multipole parts of the incident wave.⁵²

Now we examine a lossless MoS₂ disk with an eccentric hole, i.e., with the imaginary parts $\varepsilon_{\perp}^{(I)} = \varepsilon_{\parallel}^{(I)} = 0$ and with the bianisotropic response. As it was discussed above, we chose $H = R_2$, $R_2 = 258$ nm, $R_1 = 82$ nm, $\Delta_y = 98$ nm and calculate the polarizabilities α_{zz}^{mm} , and $\alpha_{zz}^{mm(x)}$, $\alpha_{zz}^{mm(y)}$ of disk according with (7a). The forms of the curves for the real and imaginary parts of $1/\alpha_{zz}^{mm}$, and $1/\alpha_{zz}^{mm(x)}$, and $1/\alpha_{zz}^{mm(y)}$ shown in Figure 4b remain qualitatively same as in Figure 3. However, due to the bianisotropy induced by the hole shift, the resonance condition $\text{Re}(1/\alpha_{zz}^{mm}) = 0$ is realized at new wavelength $\lambda \approx 1562$ nm (Figure 4b). Note that $\text{Re}(1/\alpha_{zz}^{mm(x)}) = 0$ and $\text{Re}(1/\alpha_{zz}^{mm(y)}) = 0$ are also realized at this wavelength.

Thus, the considered anisotropic disk with an eccentric hole demonstrates the bianisotropic response in the IR range. It can be used as a building block for creation of a metasurface supporting a QTM in a given spectral range. Choosing the wavelength $\lambda_{QTM} = 1552$ nm, at which a QTM is assumed to be realized, and taking $\text{Re}(1/\alpha_{zz}^{mm})$ at this wavelength (Figure 4b) we obtain from the solution of Equation (10) the period $P = 1063$ nm of the metasurface. Note that the chosen combination of the wavelength of the incident wave and the cylinder's size corresponds to the region of strong bianisotropic response m_z in Figure 4a.

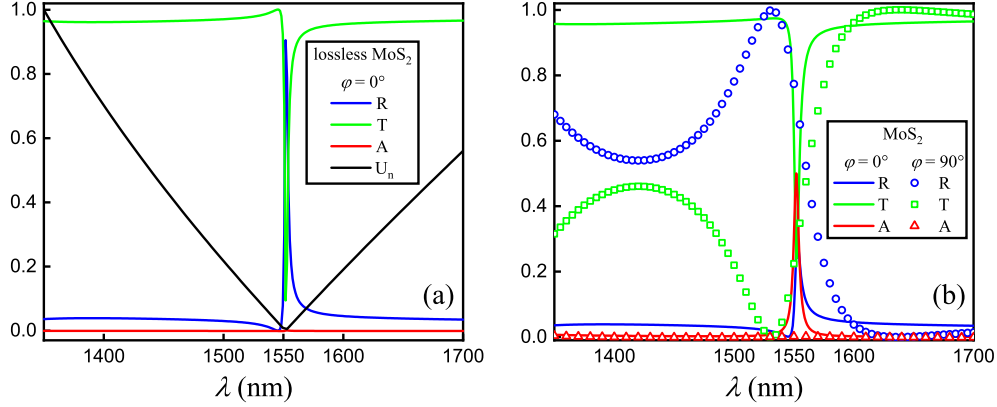


Figure 5: Spectra of the reflection (R), transmission (T), absorption (A) coefficients and parameter U_n for array with period $P = 1063$ nm composed of (a) ideal lossless and (b) real weakly-absorbing MoS₂ disks; $U_n = U/\max(U)$, where $U = |S_z^{(R)} - \text{Re}(1/\alpha_{zz}^{mm})|$; the condition $U_n = 0$ indicates the position of QTM. The geometric disk parameters correspond to Figure 4b. The angle φ determines the electric polarization of the incident waves: $\varphi = 0^\circ$ ($\varphi = 90^\circ$) determines the $E_x(E_y)$ -polarization.

This situation should guarantee a finite width of the QTM resonance because, in this case, $\text{Im}(S_z) > \text{Im}(1/\alpha_{zz}^{mm})$.

For the verification of the dipole approximation we numerically calculated, using COM-SOL, the transmission and reflection spectra of the metasurface (Figure 1a) composed of the hollow disks with the size parameters as in Figure 4 and with the period $P \approx 1063$ nm. As it is demonstrated in Figure 5a for the lossless case, the transmission and reflection spectra have narrow resonant features just at the wavelength 1552 nm of the QTM. As it is followed from the dipole approximation,³⁴ at this spectral region the strong resonant m_z component of the every disk is excited due to the realization of the QTM conditions. Simultaneously, owing to bianisotropy there is also connection m_z with p_x ,³⁴ so that the electric dipole component p_x of the every disk is also resonantly increased resulting in suppression of the transmission and increasing of reflection. Thus this behaviour is fully agreed with considerations provided by the dipole approximation. Note that the resonant values of m_z under QTM conditions lead to an increase in the near field in the metasurface plane, since disks do not emit electromagnetic waves perpendicular to this plane.³⁴

Further, we will take into account that MoS₂ has small but finite values of the imaginary parts of its dielectric permittivities in the telecommunication range (Figure 1d). As a result the absorption effect has to be realized in the metasurface with parameters as in Figure 5a and with actual MoS₂ dielectric permittivity. Results of the transmission, reflection and absorption spectra simulations for the two different polarization of the incident waves are shown in Figures. 5b. Remarkably, that for the E_x -polarization, the joint occurrence of dissipative effects in each building block and the collective effects of the QTM formation in the entire metasurface leads to the appearance of a narrow peak of collective losses at the wavelength of the QTM, see Figure 5b. This is due to the considerable concentration of the electric field inside the cylinders under the QTM conditions. Indeed, the coupling between individual cylinders in the array occurs due to the interaction of their magnetic fields. They are significantly enhanced in the holes and induce the electric field hot spots inside the cylinders, which are the centers of collective absorption, see Figure 7. This allows to use such a dissipative metasurface for ultra-narrowband absorbing in IR range or for highly sensitive detection of nanoobjects near it. Analyzing the absorptionmagentaproperties of the system, we found that under the selected conditions in Figure 5b, the absorption efficiency is high and equals to 51% at $\lambda_{QTM} = 1552$ nm. The quality factor $Q = \lambda/\text{FWHM}$ is 310 for the FWHM of absorption peak equals only to 5 nm. In addition, the system demonstrates a high $S = 380$ nm/RIU sensitivity to the environment and reaches the level of figure of merit (FOM) $\text{FOM} = 76$, compare with Refs. 3,4,18,53. Here we used the relations $S = \Delta\lambda/\Delta n$ and $\text{FOM} = S/\text{FWHM}$, where $\Delta\lambda$ is the wavelength shift of reflectance resonance as result of the environment refractive index Δn variation.

Another feature of the metasurface composed of the bianisotropic MoS₂ disks is a high polarization sensitivity. When the electric field polarization of the incident wave is rotated by an angle $\varphi = \pm 90^\circ$ the QTM, including the collective dissipative effect, completely disappears after the vanishing of the longitudinal bianisotropy of the magnetic type, see the transmission, reflection, and absorption spectra in Figure 5b calculated for $\varphi = 90^\circ$. Here φ

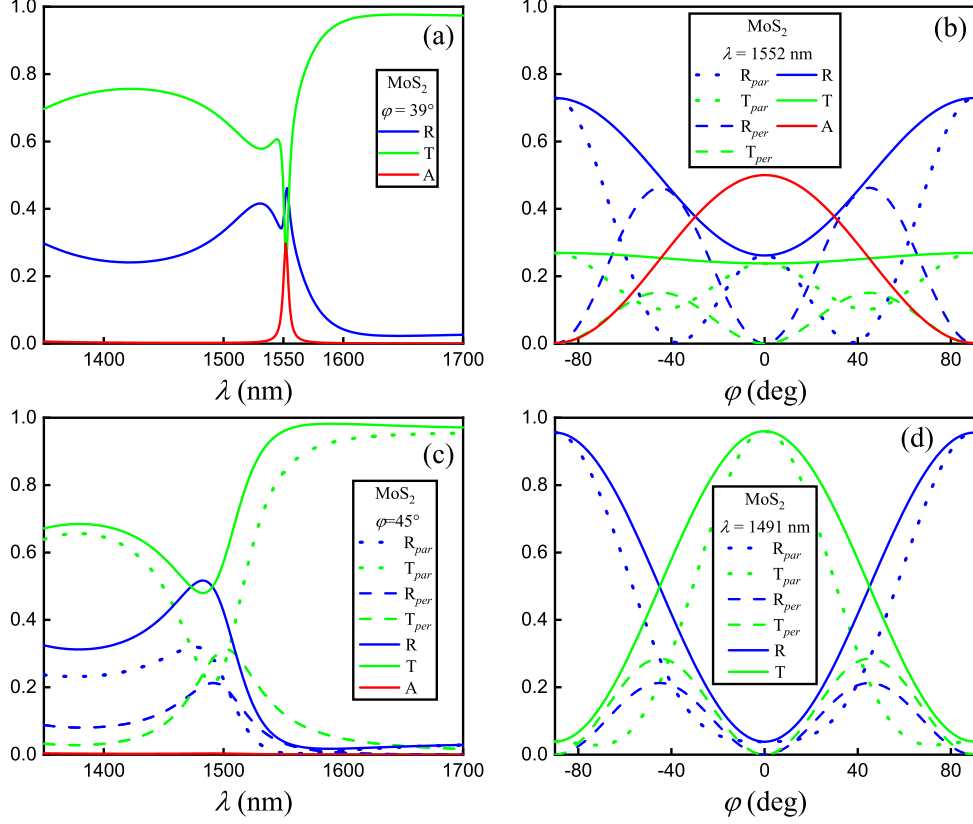


Figure 6: Spectral and angular dependencies for the total reflection (R), transmission (T) and absorption (A) coefficients and their collinear (R_{par} , T_{par}) and orthogonal (R_{per} , T_{per}) polarization components of the incident wave for array with period $P = 1063$ nm of absorbing MoS₂ disks with (a), (b) shifted hole and parameters corresponding to Figure 4b and with (c), (d) centered hole and parameters corresponding to Figure 3. The angle φ determines orientation of the electric polarization of the incident waves with respect to x -axis.

is the rotation angle in the xy -plane of the electric polarization relative to the x -axis: $\varphi = 0^\circ$ ($\varphi = 90^\circ$) corresponds to the $E_x(E_y)$ -polarization.

In addition, we investigated the polarization sensitivity over the entire range of angle φ at the wavelength $\lambda_{QTM} = 1552$ nm and found the decreasing of the absorption maximum associated with the QTM with changing the angle φ from 0° to $\pm 90^\circ$. For the case $\varphi = 39^\circ$ the result is shown in Figure 6a. Note that the spectral position of the absorption maximum does not depend on the angle φ always remaining at the wavelength $\lambda_{QTM} = 1552$ nm. The dependence of the transmission, reflection, and absorption coefficients on the angle φ at this wavelength is shown in Figure 6b. From this figure, we observe another feature: the

rotation of the polarization of the normally incident wave initiates the process of transferring part of its energy into the components of the transmitted and reflected waves, which are orthogonal to the polarization of the incident wave. In particular, choosing the angle $\varphi = 39^\circ$ leads to the generation of the reflected wave only with linear polarization that is orthogonal to the polarization of the incident wave, see curve R_{per} in Figure 6b. The maximum of the energy transformation into orthogonal component simultaneously the transmitted and reflected waves is realized at the angle $\varphi = 45^\circ$ for both parameters R_{per} and T_{per} (Figure 6b).

In order to exclude any influence of the particle bianisotropy on the cross-polarization effect in the transmission and reflection, we analyzed this effect for the metasurface composed of disks with centered holes and also found its presence in the system, see Figure 6c,d. However, in this case, the maximum for R_{per} is realized at the wavelength 1491 nm (see Figure 6c). Figure 6d, plotted for this wavelength, demonstrates the conservation of the angular position of the maximum for R_{per} (T_{per}) at $\varphi = 45^\circ$. Our simulations of the metasurfaces, composed of the disks with similar geometry fabricated from isotropic material, showed that such metasurfaces does not possess the property of polarization transformation. Thus, we can conclude that the observed effects are associated with the anisotropic properties of single building blocks. Hence, metasurfaces of subwavelength thickness composed of single in-plane symmetric building blocks of anisotropic materials can have properties of a solid plate consisting of birefringent material.

In the final part of the article we note another important feature of the quasi-trapped modes in the metasurface of anisotropic NPs. This is the presence of the preferred direction of the interaction between them. Figure 7 shows the distribution patterns of the electric (by colormap on the cylinder surface in Figures a,b and by vectors in the chosen plane in Figures c,d) and magnetic (by vectors in the chosen plane in Figures a,b and by colormap on the cylinder surface in Figures c,d) fields for the disks in metasurface plotted for different views. It can be seen that a strong coupling between single disks is realized by connecting the magnetic field lines in the zx -plane, see Figure 7a. At the same time, the magnetic field

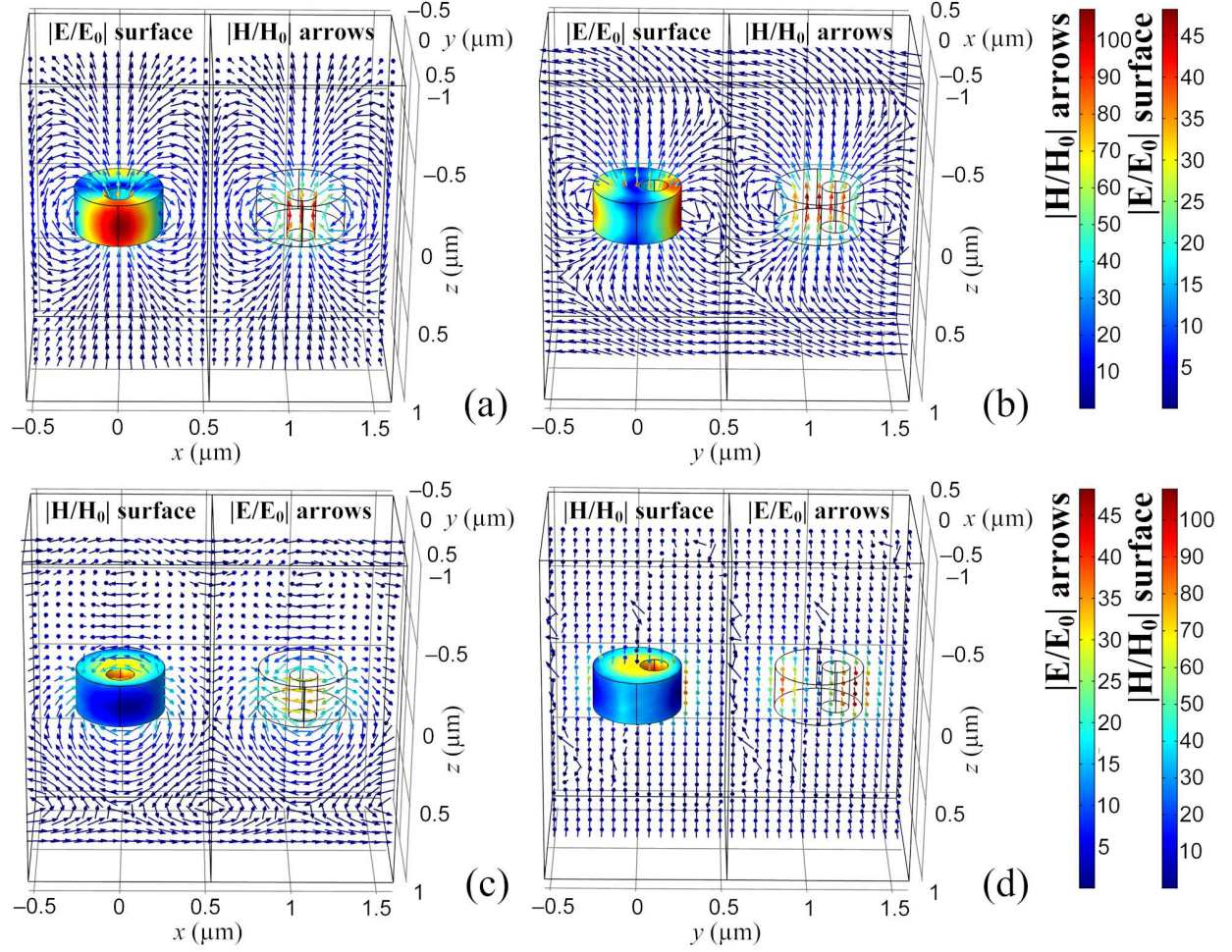


Figure 7: The visualization of electric and magnetic field distributions calculated (a), (c) in the xz -plane and (b), (d) in the yz -plane for a pair of MoS₂ disks in the metasurface at the conditions of the QTM. The metasurface parameters correspond to Figure 5a.

is tighten and concentrated in the holes of the disks with the formation of hot spots of the electric field in the narrow waist near them. On the contrary, the visualization of the magnetic field lines in the yz -plane demonstrates their distancing or “anticouplin”, see Figure 7b. A similar character of coupling/anticoupling is observed for the vectors of electric field in the space between the cylinders in Figure 7c,d. We figured out that such an asymmetric field distribution does not depend on the way of same QTM excitation, but is a particular feature of the using anisotropic materials for fabricating metasurfaces. In particular, the same character of the coupling is kept in the case of shifting the hole along x -axis and using the field $E = (0, E_y, 0) \exp(ikz)$ for irradiation of array of disks with holes.

3 Conclusion

In present work, we have studied the features of the optical response of disk NPs fabricated from an optically anisotropic material MoS₂. The scattering cross sections for different irradiation directions have been calculated. It has been shown that spectral positions of multipole resonances are determined not only the shape and size of the scatterer but also the internal material anisotropy which can affect nonlocal optical properties of the scatterers. We have investigated the features of transmission and reflection spectra of metasurfaces composed of such nanoparticles and determined conditions for the excitation of QTM leading to formation of a narrow absorption band in the telecom spectral range. It has been also found the effect of the polarization transformation leading to the appearance of reflection and transmission waves with the orthogonal polarization with respect to the polarization of the incident wave. The important role of the material anisotropy in these transformations has been demonstrated. The obtained results can be used for the design of all-dielectric metasurfaces intended for narrow-band quenching of IR signals and fabrication of polarization-sensitive distributed sensors and polarization metacoatings.

Acknowledgement

This work was supported by the Russian Science Foundation, Grant No. 20-12-00343.

References

- (1) Pendry, J. B.; Holden, A. J.; Stewart, W. J.; Youngs, I. Extremely Low Frequency Plasmons in Metallic Mesostructures. Phys. Rev. Lett. **1996**, 76, 4773.
- (2) Liu, J.-P.; Zhai, X.; Wang, L.-L.; Li, H.-J.; Xie, F.; Xia, S.-X.; Shang, X.-J.; Luo, X. Graphene-based long-range SPP hybrid waveguide with ultra-long propagation length in mid-infrared range. Opt. Express **2016**, 24, 5376–5386.

- (3) Shen, Y.; Zhou, J.; Liu, T.; Tao, Y.; Jiang, R.; Liu, M.; Xiao, G.; Zhu, J.; Zhou, Z.-K.; Wang, X.; Jin, C.; Wang, J. Plasmonic gold mushroom arrays with refractive index sensing figures of merit approaching the theoretical limit. Nat. Commun. **2013**, 4, 2381.
- (4) Wu, D.; Li, R.; Liu, Y.; Yu, Z.; Yu, L.; Chen, L.; Liu, C.; Ma, R.; Ye, H. Ultra-narrow Band Perfect Absorber and Its Application as Plasmonic Sensor in the Visible Region. Nanoscale Res. Lett. **2017**, 12, 427.
- (5) Kuznetsov, S. A.; Paulish, A. G.; Gelfand, A. V.; Lazorskiy, P. A.; Fedorinin, V. N. Bolometric THz-to-IR converter for terahertz imaging. Appl. Phys. Lett. **2011**, 99, 023501.
- (6) Yan, D.; Meng, M.; Li, J.; Li, X. Graphene-Assisted Narrow Bandwidth Dual-Band Tunable Terahertz Metamaterial Absorber. Front. Phys. **2020**, 8, 306.
- (7) Wu, X.; Jiang, P.; Razinskas, G.; Huo, Y.; Zhang, H.; Kamp, M.; Rastelli, A.; Schmidt, O. G.; Hecht, B.; Lindfors, K.; Lippitz, M. On-Chip Single-Plasmon Nanocircuit Driven by a Self-Assembled Quantum Dot. Nano Lett. **2017**, 17, 4291–4296.
- (8) Stebunov, Y. V.; Aftenieva, O. A.; Arsenin, A. V.; Volkov, V. S. Highly Sensitive and Selective Sensor Chips with Graphene-Oxide Linking Layer. ACS Appl. Mater. Interfaces **2015**, 7, 21727–21734.
- (9) Shi, L.; Shang, J.; Liu, Z.; Li, Y.; Fu, G.; Liu, X.; Pan, P.; Luo, H.; Liu, G. Ultra-narrow multi-band polarization-insensitive plasmonic perfect absorber for sensing. Nanotechnology **2020**, 31, 465501.
- (10) Wu, D.; Liu, Y.; Li, R.; Chen, L.; Ma, R.; Liu, C.; Ye, H. Infrared Perfect Ultra-narrow Band Absorber as Plasmonic Sensor. Nanoscale Res. Lett. **2016**, 11, 483.
- (11) Lu, X.; Wan, R.; Zhang, T. Metal-dielectric-metal based narrow band absorber for sensing applications. Opt. Express **2015**, 23, 29842–29847.

- (12) Evlyukhin, A. B.; Reinhardt, C.; Seidel, A.; Luk'yanchuk, B. S.; Chichkov, B. N. Optical response features of Si-nanoparticle arrays. Physical Review B **2010**, 82, 045404.
- (13) Offermans, P.; Schaafsma, M. C.; Rodriguez, S. R. K.; Zhang, Y.; Crego-Calama, M.; Brongersma, S. H.; Gómez Rivas, J. Universal scaling of the figure of merit of plasmonic sensors. ACS nano **2011**, 5, 5151–5157.
- (14) Evlyukhin, A. B.; Reinhardt, C.; Zywiets, U.; Chichkov, B. N. Collective resonances in metal nanoparticle arrays with dipole-quadrupole interactions. Phys. Rev. B **2012**, 85, 245411.
- (15) Babicheva, V. E.; Evlyukhin, A. B. Resonant lattice Kerker effect in metasurfaces with electric and magnetic optical responses. Laser & Photonics Reviews **2017**, 11, 1700132.
- (16) Kravets, V. G.; Kabashin, A. V.; Barnes, W. L.; Grigorenko, A. N. Plasmonic surface lattice resonances: a review of properties and applications. Chemical reviews **2018**, 118, 5912–5951.
- (17) Cherqui, C.; Bourgeois, M. R.; Wang, D.; Schatz, G. C. Plasmonic surface lattice resonances: Theory and computation. Accounts of chemical research **2019**, 52, 2548–2558.
- (18) Fan, K.; Suen, J. Y.; Liu, X.; Padilla, W. J. All-dielectric metasurface absorbers for uncooled terahertz imaging. Optica **2017**, 4, 601–604.
- (19) Yang, C.-Y.; Yang, J.-H.; Yang, Z.-Y.; Zhou, Z.-X.; Sun, M.-G.; Babicheva, V. E.; Chen, K.-P. Nonradiating Silicon Nanoantenna Metasurfaces as Narrowband Absorbers. ACS Photonics **2018**, 5, 2596–2601.
- (20) Wang, Y.; Zhu, D.; Cui, Z.; Hou, L.; Lin, L.; Qu, F.; Liu, X.; Nie, P. All-Dielectric Terahertz Plasmonic Metamaterial Absorbers and High-Sensitivity Sensing. ACS Omega **2017**, 4, 601–604.

- (21) Wang, Y.; Yue, L.; Cui, Z.; Zhang, X.; Zhang, X.; Zhu, Y. Q.; Zhang, K. Optically tunable single narrow band all-dielectric terahertz metamaterials absorber. AIP Adv. **2020**, 10, 045039.
- (22) Tian, J.; Luo, H.; Li, Q.; Pei, X.; Du, K.; Qiu, M. Near-Infrared Super-Absorbing All-Dielectric Metasurface Based on Single-Layer Germanium Nanostructures. Laser Photonics Rev. **2018**, 12, 1800076.
- (23) Gubin, M. Y.; Shesterikov, A. V.; Prokhorov, A. V.; Volkov, V. S. Hybrid Schemes for Excitation of Collective Resonances with Surface Plasmon Polaritons in Arrays of Quantum Dots in the Proximity of Graphene. Laser Photonics Rev. **2020**, 14, 2000237.
- (24) Zhang, J.; MacDonald, K. F.; Zheludev, N. I. Near-infrared trapped mode magnetic resonance in an all-dielectric metamaterial. Optics express **2013**, 21, 26721–26728.
- (25) Tuz, V. R.; Khardikov, V. V.; Kivshar, Y. S. All-dielectric resonant metasurfaces with a strong toroidal response. ACS Photonics **2018**, 5, 1871–1876.
- (26) Mackay, T. G.; Lakhtakia, A. Electromagnetic anisotropy and bianisotropy: a field guide; World Scientific Publishing Co. Pte. Ltd., 2009.
- (27) Koshelev, K.; Bogdanov, A.; Kivshar, Y. Meta-optics and bound states in the continuum. Sci. Bull. **2019**, 64, 836–842.
- (28) Monticone, F.; Sounas, D.; Krasnok, A.; Alù, A. Can a Nonradiating Mode Be Externally Excited? Nonscattering States versus Embedded Eigenstates. ACS Photonics **2019**, 6, 3108–3114.
- (29) Abujetas, D. R.; van Hoof, N.; ter Huurne, S.; Rivas, J. G.; Sánchez-Gil, J. A. Spectral and temporal evidence of robust photonic bound states in the continuum on terahertz metasurfaces. Optica **2019**, 6, 996–1001.

- (30) Li, S.; Zhou, C.; Liu, T.; Xiao, S. Symmetry-protected bound states in the continuum supported by all-dielectric metasurfaces. Phys. Rev. A **2019**, 100, 063803.
- (31) Han, S.; Pitchappa, P.; Wang, W.; Srivastava, Y. K.; Rybin, M. V.; Singh, R. Extended Bound States in the Continuum with Symmetry-Broken Terahertz Dielectric Metasurfaces. Adv. Opt. Mater. **2021**, 9, 2002001.
- (32) Fedotov, V.; Rose, M.; Prosvirnin, S.; Papasimakis, N.; Zheludev, N. Sharp trapped-mode resonances in planar metamaterials with a broken structural symmetry. Physical review letters **2007**, 99, 147401.
- (33) Tuz, V. R.; Khardikov, V. V.; Kupriianov, A. S.; Domina, K. L.; Xu, S.; Wang, H.; Sun, H.-B. High-quality trapped modes in all-dielectric metamaterials. Opt. Express **2018**, 26, 2905–2916.
- (34) Evlyukhin, A. B.; Tuz, V. R.; Volkov, V. S.; Chichkov, B. N. Bianisotropy for light trapping in all-dielectric metasurfaces. Phys. Rev. B **2020**, 101, 205415.
- (35) Xu, L.; Kamali, K. Z.; Huang, L.; Rahmani, M.; Smirnov, A.; Camacho-Morales, R.; Ma, Y.; Zhang, G.; Woolley, M.; Neshev, D.; Miroshnichenko, A. E. Dynamic Nonlinear Image Tuning through Magnetic Dipole Quasi-BIC Ultrathin Resonators. Adv. Sci. **2019**, 6, 1802119.
- (36) Kamali, K. Z.; Xu, L.; Ward, J.; Wang, K.; Li, G.; Miroshnichenko, A. E.; Neshev, D.; Rahmani, M. Reversible Image Contrast Manipulation with Thermally Tunable Dielectric Metasurfaces. Small **2019**, 15, 1805142.
- (37) Novoselov, K. S.; Mishchenko, A.; Carvalho, A.; Neto, A. H. C. 2D materials and van der Waals heterostructures. Science **2016**, 353, aac9439.
- (38) Ermolaev, G. A. et al. Giant optical anisotropy in transition metal dichalcogenides for next-generation photonics. Nat. Commun. **2021**, 12, 854.

- (39) Chhowalla, M.; Shin, H. S.; Eda, G.; Li, L.-J.; Loh, K. P.; Zhang, H. The chemistry of two-dimensional layered transition metal dichalcogenide nanosheets. Nat. Chem. **2013**, 5, 263–275.
- (40) Schönfeld, B.; Huang, J.; Moss, S. Anisotropic mean-square displacements (MSD) in single-crystals of 2H- and 3R-MoS₂. Acta Cryst. B **1983**, 39, 404–407.
- (41) Ermolaev, G. A.; Stebunov, Y. V.; Vyshnevyy, A. A.; Tatarkin, D. E.; Yakubovsky, D. I.; Novikov, S. M.; Baranov, D. G.; Shegai, T.; Nikitin, A. Y.; Arsenin, A. V.; Volkov, V. S. Broadband optical properties of monolayer and bulk MoS₂. npj 2D Materials and Applications **2020**, 4, 21.
- (42) Yoffe, A. D. Layer Compounds. Annu. Rev. Mater. Sci. **1973**, 3, 147–170.
- (43) Evlyukhin, A. B.; Chichkov, B. N. Multipole decompositions for directional light scattering. Phys. Rev. B **2019**, 100, 125415.
- (44) Varault, S.; Rolly, B.; Boudarham, G.; Demésy, G.; Stout, B.; Bonod, N. Multipolar effects on the dipolar polarizability of magneto-electric antennas. Optics express **2013**, 21, 16444–16454.
- (45) Asadchy, V. S.; Díaz-Rubio, A.; Tretyakov, S. A. Bianisotropic metasurfaces: physics and applications. Nanophotonics **2018**, 7, 1069–1094.
- (46) Achouri, K.; Martin, O. J. Extension of Lorentz Reciprocity and Poynting Theorems for Spatially Dispersive Media with Quadrupolar Responses. arXiv preprint arXiv:2102.08197 **2021**,
- (47) Bobylev, D. A.; Smirnova, D. A.; Gorlach, M. A. Nonlocal response of Mie-resonant dielectric particles. Physical Review B **2020**, 102, 115110.

- (48) Evlyukhin, A. B.; Reinhardt, C.; Chichkov, B. N. Multipole light scattering by non-spherical nanoparticles in the discrete dipole approximation. Physical Review B **2011**, 84, 235429.
- (49) Staude, I.; Miroshnichenko, A. E.; Decker, M.; Fofang, N. T.; Liu, S.; Gonzales, E.; Dominguez, J.; Luk, T. S.; Neshev, D. N.; Brener, I., et al. Tailoring directional scattering through magnetic and electric resonances in subwavelength silicon nanodisks. ACS nano **2013**, 7, 7824–7832.
- (50) Babicheva, V. E.; Evlyukhin, A. B. Multipole lattice effects in high refractive index metasurfaces. Journal of Applied Physics **2021**, 129, 040902.
- (51) Evlyukhin, A. B.; Poleva, M.; Prokhorov, A.; Baryshnikova, K.; Miroshnichenko, A. E.; Chichkov, B. N. Polarization switching of quasi-trapped modes and near field enhancement in bianisotropic all-dielectric metasurfaces. arXiv:2108.02195 **2021**,
- (52) Varault, S.; Rolly, B.; Boudarham, G.; Demésy, G.; Stout, B.; Bonod, N. Multipolar effects on the dipolar polarizability of magneto-electric antennas. Opt. Express **2013**, 21, 16444–16454.
- (53) Wang, Y.; Yue, L.; Cui, Z.; Zhang, X.; Zhang, X.; Zhu, Y.; Zhang, K. Optically tunable single narrow band alldielectric terahertz metamaterials absorber. AIP Adv. **2020**, 10, 045039.

Graphical TOC Entry

